21st Australasian Fluid Mechanics Conference
Adelaide, Australia
10-13 December 2018

Numerical Study of a NACA0015 Circulation Control Aerofoil Using Synthetic Jets

P. Itsariyapinyo and R.N. Sharma

Department of Mechanical Engineering
University of Auckland, Auckland 1142, New Zealand

Abstract

Large eddy simulation of a NACA0015 circulation control aerofoil using synthetic jets is presented in this paper. In its usual appearance, the circulation control aerofoil features a rounded trailing edge (Coanda surface) which attracts an air jet provided upstream to modify the aerodynamic coefficients on the aerofoil. A chord Reynolds number of 1.10×10^5, excitation frequency of 175 Hz, momentum coefficients of 0.0044 to 0.0688, and angles of attack of 0°, 6°, and 12° are employed in this study. Fluctuations in the lift and drag coefficients on the non-actuated aerofoil are found to be governed by the vortex shedding frequency. Provided that the momentum coefficient is sufficiently high, the lift and drag coefficients tend to fluctuate at the synthetic jet frequency. The mean lift coefficient linearly increases with the momentum coefficient at a low momentum coefficient range and its incremental rate begins to decline at a high momentum coefficient range. Increasing the angle of attack of the aerofoil is observed to slightly reduce the slope of the lift increment.

Introduction

In the past decades, the circulation control aerofoil has attracted much research attention due to its promising application as a high-lift device [1]. The circulation control aerofoil, in general, consists of an air plenum, an orifice, and a rounded trailing edge (Coanda surface) which is designed to facilitate the Coanda effect. In order to induce the Coanda effect, compressed air is usually either supplied from a compressor or a propulsive system to force an air jet through an orifice. Upon forcing an air jet onto the Coanda surface, additional momentum provided by an air jet reenergises the local shear flow which enables the flow to remain attached on the Coanda surface for a longer angular distance and ultimately modifies the aerodynamic coefficients on the aerofoil.

Despite the circulation control aerofoil being used in actual flights [1], its reliance on the additional plumbing system and a continuous air jet further complicates the flight control system and reduces the opportunity to exploit flow instabilities on the aerofoil (e.g. vortex shedding). Unlike the conventional circulation control aerofoil which makes use of a continuous air jet, a synthetic jet actuator consists of an orifice, an oscillating membrane, and a cavity. Since an oscillating membrane, such as a loudspeaker and a piezoelectric membrane, is normally driven by a series of sinusoidal waves, successive suction and blowing can be produced from the ingestion and expulsion strokes which take place when an oscillating membrane oscillates outward and inward, respectively. Hence, a synthetic jet actuator is also known as a "zero-net-mass-flux" (ZNMF) device.

The objective of the current study is to explore the effects of synthetic jet actuation on the aerodynamic characteristics of the aerofoil through spectral analysis, statistical analysis, and flow visualisation. Since the effects of excitation frequency on the aerodynamic coefficients have been investigated to a certain extent in the experimental study of the same aerofoil [2], the current study will focus more on the effects of the momentum coefficient as the synthetic jet actuators used in the experimental study provide relatively low momentum coefficient. Thus, the excitation frequency of 175 Hz (Sr = 0.14), momentum coefficients of 0.0044 to 0.0688, and angles of attack of 0°, 6°, and 12° are employed in this numerical study.

Numerical Setup

The design of the circulation control aerofoil is based on Englar's hypothesis [3] which yields the ratios of the jet height to the Coanda radius (b/r), the jet height to the aerofoil chord length (b/c), and the Coanda radius to the aerofoil chord length (r/c) of 0.05, 0.0012, and 0.0235, respectively. The designations for the geometrical parameters b, c, and r can be referred to Figures 1a and c. In order to maintain consistency between the experimental and numerical studies, a free-stream velocity and aerofoil chord length of 10 m/s and 170 mm are employed to yield a chord Reynolds number of 1.10×10^5, respectively. The geometries and meshes of the flow domain are created in ICEM CFD 15.0 using an unstructured hexahedral mesh. Pre-CFX, CFX Solver, and Post-CFD of ANSYS CFD R15.0 Academic edition are used to produce numerical results.

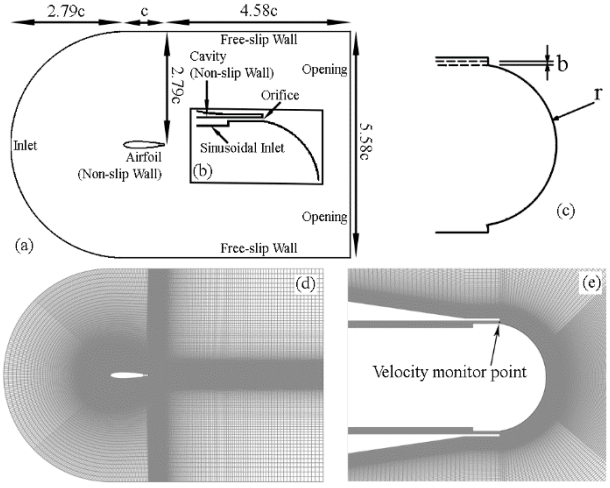

Figure 1. Boundary conditions of (a) a flow domain and (b) the synthetic jet actuator, (c) the schematics of the Coanda surface, and the meshing topology around (d) the aerofoil and (e) the rounded trailing edge.

The C-grid configuration, as shown in Figures 1a, b, and d, is employed for this simulation. The round arc with a radius of 2.79c is assigned as an inlet and prescribed with a free-stream velocity. The vertical distance from the top to bottom walls of the flow domain is 5.58c. The top and bottom walls are assigned free-slip walls. The streamwise distance from the trailing edge to the far-end wall is 4.58c. The far-right wall is assigned as an opening. The surfaces of the aerofoil, orifice, and the cavity are assigned as non-slip walls. The side walls of this flow domain are assigned as symmetry planes. The aerofoil span length of 0.07c is used in the simulation as it is found to be capable of

resolving the turbulent coherence structure on an aerofoil while optimizing the computational time. The oscillating membrane is modelled as a sinusoidal velocity inlet whose amplitude is defined by the form $U_j\ (t) = U_d \sin(2\pi ft)$ where U_d is the membrane velocity and f is the excitation frequency. The value of the synthetic jet velocity at the orifice (U_j), which is used to estimate the momentum coefficient, was obtained from the monitor point which is placed at the orifice exit (see Figure 1e). In order to be able to resolve the near-wall flow, the y^+ value for the first near-wall node is kept slightly below 1. In this paper, LES (WALES), central difference advection scheme, and second order backward Euler transient scheme are used to solve for the results. While the validation of the numerical results is not presented here due to the page limit, it is noted that the differences in the dominant frequencies, the lift coefficients, and the drag coefficients between the experimental [2] and numerical studies are typically below 10%, 2%, and 5%, respectively.

In this study, the vortex shedding and synthetic jet frequencies are normalised by the diameter of the Coanda surface d and a free-stream velocity U_∞ to yield the Strouhal number Sr.

$$Sr = fd/U_\infty \tag{1}$$

In an attempt to establish a measure for the synthetic jet momentum so that the numerical results could be validated with the experimental results, the formula for the synthetic jet momentum coefficient is expressed as

$$C_\mu = \frac{\bar{I}_j}{1/2\,\rho_\infty U_\infty^2 c} \tag{2}$$

$$\bar{I}_j = \frac{1}{T/2}\rho_j b \int_0^{T/2} U_j^2(t)dt \tag{3}$$

where $\bar{I}_j$ is the time-averaged jet momentum per unit length during the expulsion stroke, T is the actuation period or the reciprocal of the actuation frequency f, ρ_j is the air density, U_j is the jet velocity at the exit of the slot of the actuator, b is the width or height of the jet slot, ρ_∞ is the free-stream density, U_∞ is a free-stream velocity, and c is the chord length.

Results

Fluctuations in Lift and Drag Coefficients of Baseline Cases

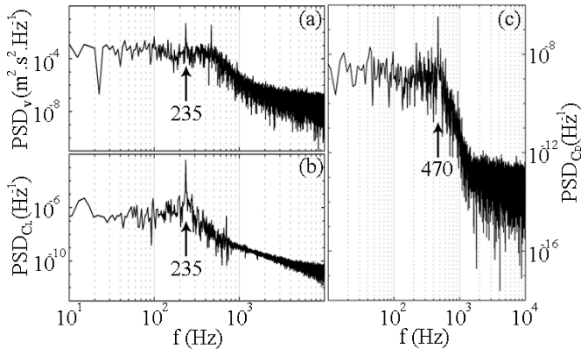

Figure 2. Spectra of (a) fluctuating y-direction velocities, (b) fluctuating lift coefficients, and (c) fluctuating drag coefficients on the non-actuated aerofoil at α = 0°.

Figures 2, 3, and 4 show the spectra of fluctuating y-direction velocities (v), fluctuating lift coefficients (C_L), and fluctuating drag coefficients (C_D) on the aerofoil at α = 0°, 6°, and 12°, respectively. In order to verify that the lift coefficient actually fluctuates at or close to the vortex shedding frequency, the spectra of fluctuating lift coefficients are plotted against those of y-direction velocities.

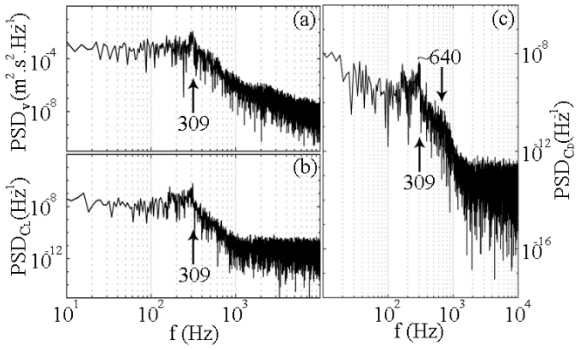

Figure 3. Spectra of (a) fluctuating y-direction velocities, (b) fluctuating lift coefficients, and (c) fluctuating drag coefficients on the non-actuated aerofoil at α = 6°.

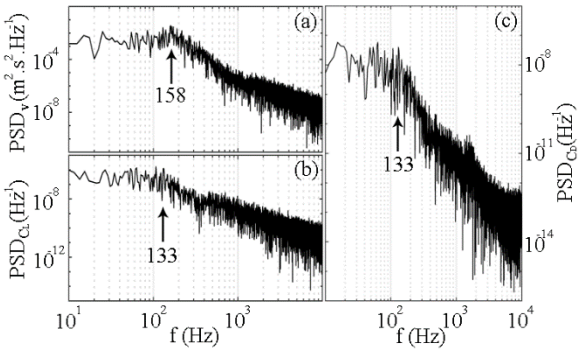

Figure 4. Spectra of (a) fluctuating y-direction velocities, (b) fluctuating lift coefficients, and (c) fluctuating drag coefficients on the non-actuated aerofoil at α = 12°.

The results show good agreement between the fluctuating lift frequencies and the vortex shedding frequencies for all angles of attack in which the fluctuating lift frequencies are identical or similar to the vortex shedding frequencies. Similar to other investigations on a circular cylinder [4], it is evident from the spectra of fluctuating drag coefficients at α = 0° (Figure 2c) that the drag coefficient fluctuates at twice the fluctuating lift frequency. However, at α = 6° and 12°, the fluctuating drag frequencies (Figures 3c and 4c) are equal or similar to their respective vortex shedding frequencies.

Fluctuations in Lift and Drag Coefficients of Actuated Cases

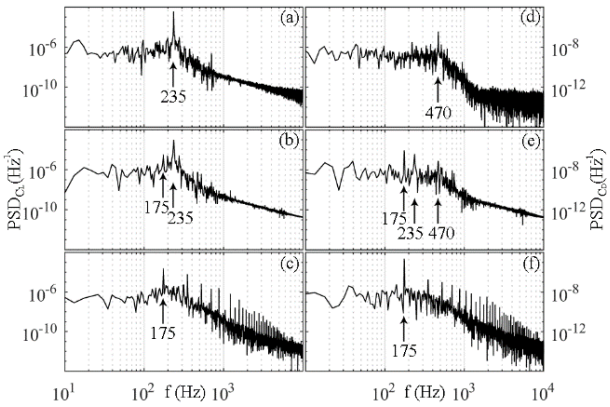

Figure 5. Spectra of flucutating lift coefficients on (a) the non-actauted aerofoil and actuated aerofoil when C_μ = (b) 0.0044 and (c) 0.0688 and spectra of flucutating drag coefficients on (d) the non-actauted aerofoil and actuated aerofoil when C_μ = (e) 0.0044 and (f) 0.0688.

Since the fluctuating lift and drag coefficients are normally governed by the vortex shedding mode when the aerofoil is not excited, it is of interest to see whether the characteristics of

these fluctuations could be modified by the synthetic jet actuation provided that the momentum coefficient is sufficiently high. In an attempt to answer the above question, spectra of fluctuating lift and drag coefficients on the non-actuated and actuated aerofoils are shown in Figure 5 to provide some insight into the effects of synthetic jet actuation on the fluctuating lift and drag frequencies. For the sake of simplicity and conciseness, only the spectra from $\alpha = 0°$ are presented. As mentioned in the previous section, the fluctuating lift and drag frequencies on the non-actuated aerofoil are characterised by the vortex shedding frequency (Figures 5a and d). Although a weak spectral peak at 175 Hz could be found on the lift spectra when a synthetic jet is actuated at $C_\mu = 0.0044$ (Figure 5b), it is noted that a spectral peak at 235 Hz which represents vortex shedding is still the dominant mode. Nevertheless, the magnitude of a spectral peak at 175 Hz on the drag spectra is observed to be higher than that of the fluctuating drag frequency which is normally twice the vortex shedding frequency (470 Hz). Additionally, the magnitude of a spectral peak at 235 Hz is observed to exceed that of a spectral peak at 470 Hz (Figure 5e). Due to the intervention of a synthetic jet, a reduction in the magnitude of a spectral peak at 470 Hz which is accompanied by an increase in the magnitude of a spectral peak at 235 Hz may occur as a result of imbalanced vorticities between the suction and pressure sides of the aerofoil. When a synthetic jet is actuated at high momentum coefficient ($C_\mu = 0.0688$), the spectral peaks at 175 Hz become very apparent on both lift and drag spectra (Figures 5c and f). Further observation reveals that their subharmonics could also be found at every increment of 175 Hz. Unlike the cases of zero (non-actuated case) and low momentum coefficients whose spectra imply that their fluctuating aerodynamic coefficients are mostly and partly governed by the vortex shedding frequency, respectively, the lift and drag spectra at a high momentum coefficient suggest that their fluctuations may be dictated by the synthetic jet frequency. In order to further explore the likeliness of this possibility, time-history profiles of fluctuating lift and drag coefficients of the non-actuated and actuated aerofoil (C_μ = 0.0044 and 0.0688) are provided for the discussion.

Figures 6a, b, c, and d are taken from $t/T_{act} = 0.25$ (expulsion stroke), 0.5, 0.75 (ingestion stroke), and 1.00 which are corresponding to t = 0.0525, 0.0539, 0.0553, and 0.0568s in Figures 6g and h, respectively. According to the lift and drag spectra when $C_\mu = 0.0044$ (Figures 5c and d), these spectra seem to suggest that fluctuations in the lift coefficients are still mostly governed by the vortex shedding mode (235 Hz) whereas the drag coefficient is observed to fluctuate at mixed frequencies of a synthetic jet (175 Hz), vortex shedding (235 Hz), and twice the vortex shedding (470 Hz). Although the synthetic jet frequency is found to be the dominant mode in the drag spectrum, evidence of the existence of vortex shedding is still quite clear from the spectra (Figure 5b) and the flow visualization. As shown in Figures 6a-d, a trail of vortices can be seen in the wake of the aerofoil and these vortices are indicated by the yellow contours and the arrows. Similar to fluctuating lift coefficients on the non-actuated aerofoil, fluctuations in the lift coefficients at $C_\mu = 0.0044$ are observed to follow the sequences of vortex shedding in which the peaks of the lift coefficient, which are obtained within $0.0525s < t < 0.0539s$ and at $t = 0.0568s$ in Figure 6g, are corresponding to vortex shedding on the pressure side of the aerofoil (Figures 6a and d) whereas the trough of the lift coefficient, which is obtained within $0.0539s < t < 0.0553s$ in Figure 6g, is corresponding to vortex shedding on the suction side of the aerofoil (Figures 6b-c). Regarding the fluctuations in the drag coefficients at $C_\mu = 0.0044$, the time-history profile of drag coefficients shows that some cycles of fluctuating drag coefficients begin to fluctuate at the synthetic jet frequency (unshaded timeframe in Figure 6h) while some other cycles continue to fluctuate at the frequencies higher than the synthetic jet frequency (blue shaded timeframe in Figure 6h).

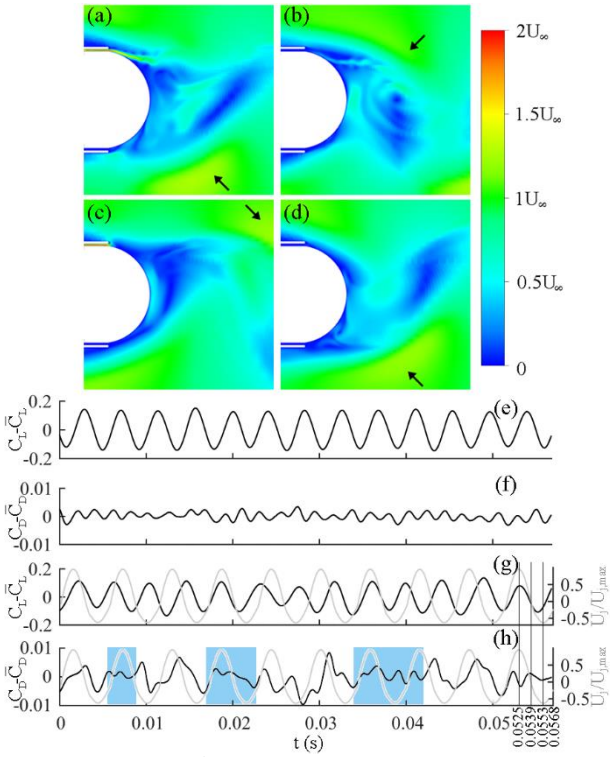

Figure 6. Sequence of the synthetic jet actuation (C_μ = 0.0044) as illustrated by contour maps of instantaneous velocity at t/T_{act} = (a) 0.25, (b) 0.50, (c) 0.75, and (d) 1.00 and fluctuating (e) lift and (f) drag coefficients on the non-actuated aerofoil and fluctuating (g) lift and (h) drag coefficients (black trend) on the actuated aerofoil at α = 0° plotted against the synthetic jet velocity profile (grey trend).

Figures 7a, b, c, and d are taken from $t/T_{act} = 0.25$ (expulsion stroke), 0.5, 0.75 (ingestion stroke), and 1.00 which are corresponding to t = 0.0353, 0.0368, 0.0381, and 0.0396s in Figures 7e and f, respectively. As opposed to the case of C_μ = 0.0044, it is evident from the spectra (Figures 5c and f) and time-history profiles of both lift and drag coefficients that fluctuations in these aerodynamic coefficients (Figures 7e and f) are dictated by the synthetic jet actuation at $C_\mu = 0.0688$. In this case where the lift and drag profiles are strongly correlated to the synthetic jet profile, the cross-correlations of the aerodynamic (lift and drag) profiles and the synthetic jet profile (Figures 7g and h) reveal that the time series of the lift and drag profiles lag behind that of the synthetic jet profile by approximately 41° and 39° (9.14×10^{-4}s), respectively. Since the lift and drag profiles at $C_\mu = 0.0688$ fluctuate at the synthetic jet frequency and their phase angles lag behind the synthetic jet profile by about 40° on the average, it is of interest that the characteristics of these consistent lift (Figure 7e) and drag (Figure 7f) waveforms are described with respect to the cycle of the synthetic jet actuation.

From $t/T_{act} = 0$ to 0.25, the trends of both lift and drag profiles are found to follow the uphill trip of the synthetic jet profile. Followed by the peak of the synthetic jet profile ($0.25 < t/T_{act} < 1.00$), the lift profile develops 2 peak values at $t/T_{act} \approx 0.30$ and 0.60 while the drag profile develops a single peak value at $t/T_{act} \approx 0.36$. Due to the fact that the synthetic jet actuation consists of successive blowing (Figure 7a) and suction (Figure 7c), 2 vortices which are produced from the orifice edge during blowing ($0 < t/T_{act} < 0.50$) and suction ($0.50 < t/T_{act} < 1.00$) are likely to be responsible for the double-peak lift profile. Followed by the peaks of both lift and drag profiles, the trend of the lift profile continues to drop during $0.60 < t/T_{act} < 1.00$

whereas that of the drag profile falls and rises as a synthetic jet undergoes its ingestion stroke at $0.50 < t/T_{act} < 0.75$ and returns to its neutral stage ($U_j/U_{j,max} = 0$) at $0.75 < t/T_{act} < 1.00$, respectively. The complete time-history profiles of these fluctuating lift and drag coefficients show that such fluctuations continue to repeat their cycles at the pace of a synthetic jet.

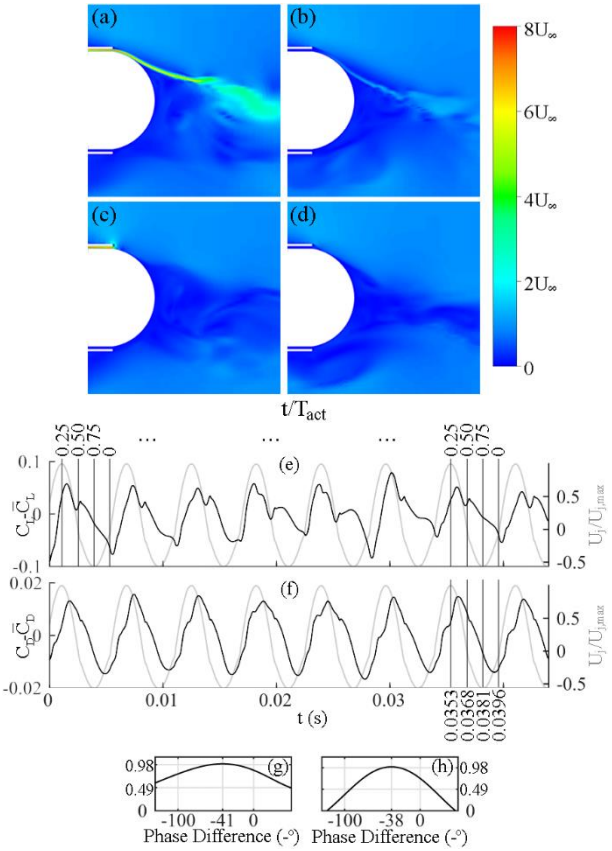

Figure 7. Sequence of the synthetic jet actuation (C_μ = 0.0688) as illustrated by contour maps of instantaneous velocity at t/T_{act} = (a) 0, (b) 0.25, (c) 0.50, and (d) 0.75, series of fluctuating (e) lift and (f) drag coefficients (black trend) on the actuated aerofoil at α = 0° plotted against the synthetic jet velocity profile (grey trend), and cross-correlations of aerodynamic coefficients ((g) lift and (h) drag coefficients) and the synthetic jet velocity profile.

Mean Lift Coefficient

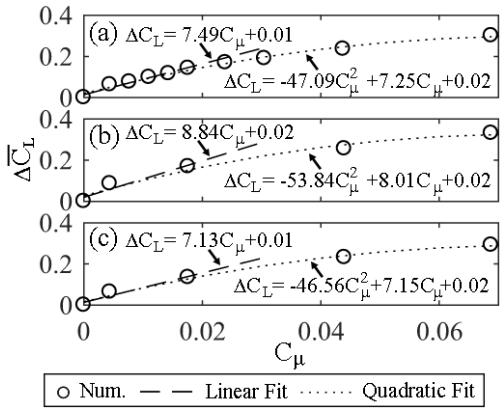

Figure 8. Effects of momentum coefficient on the incremental lift coefficient on the aerofoil at α = (a) 0°, (b) 6°, and (c) 12°.

In Figures 8a-c, dash lines and dot lines are drawn to provide linear fits to the plots at $0 < C_\mu < 0.0172$ and quadratic fits to the plots at $0 < C_\mu < 0.0688$, respectively. Although the linear fits are provided to the plots at $0 < C_\mu < 0.0172$, these linear fits are extended to $C_\mu = 0.0300$ so that the differences between the linear and quadratic fits at $C_\mu > 0.0172$ could be seen. Since the lift increment slopes at $0 < C_\mu < 0.0044$ which are estimated from the numerical study agree well with those acquired from the experimental study [2], the lift increment slopes at $0.0044 < C_\mu < 0.0688$ are further estimated from the numerical approach to explore the effects of synthetic jet actuation at higher momentum coefficients. At $0 < C_\mu < 0.0172$, the lift coefficient is observed to almost linearly increase with the momentum coefficient. Although the lift coefficient continues to increase at $0.0172 < C_\mu < 0.0688$, the rates of lift increment gradually decline as the synthetic jet actuation is approaching C_μ = 0.0688. Due to these gradual declines in the rates of lift increment at a high momentum coefficient range, a quadratic function has the best fit to these lift increment slopes. Furthermore, the quadratic fits of the lift increment slopes suggest that the effectiveness of the synthetic jet actuation may be somewhat dependent on the angle of attack as the lift increment slope slightly increases and decreases at α = 6° and 12°, respectively.

Conclusions

It is found in this study that the fluctuating lift frequency is identical or similar to the vortex shedding frequency in some cases. Interestingly, the fluctuating drag frequency of the non-actuated aerofoil at α = 0° exhibits great similarity to that of a circular cylinder in which the drag coefficient is found to fluctuate at twice the vortex shedding frequency. On the other hand, the fluctuating drag frequencies of the non-actuated aerofoil at α = 6° and 12° are identical to their fluctuating lift frequencies. Upon actuating a synthetic jet on the aerofoil, it is found that the lift and drag coefficients tend to fluctuate at the synthetic jet frequency as the momentum coefficient increases. The mean lift coefficient is found to linearly increase with the momentum coefficient at a low momentum coefficient range. Nevertheless, a further observation on the relationship between the lift coefficient and the momentum coefficient reveals that a quadratic function has the best fit for this plot as the incremental rate of the lift coefficient begins to decline at a high momentum coefficient range ($0.0172 < C_\mu < 0.0688$). The quadratic fits for the lift increment slopes also suggest that the effectiveness of the synthetic jet actuation may be somewhat dependent on the angle of attack as the lift increment slope slightly increases and decreases at α = 6° and 12°, respectively.

References

[1] Joslin, R.D., and Jones, G.S. eds., "Applications of Circulation Control Technologies," AIAA, Reston, VA, 2006.

[2] Itsariyapinyo, P., and Sharma, R.N., "Experimental Study of a NACA0015 Circulation Control Aerofoil Using Synthetic Jets," *9th Asia-Pacific Conference on Wind Engineering*, Auckland, New Zealand, 2017.

[3] Englar, R.J., "Two-Dimensional Subsonic Wind Tunnel Tests of Two 15-Percent Thick Circulation Control Airfoils. Technical Note AL-211." Bethesda, MD, 1971.

[4] Bishop, R.E.D., and Hassan, A.Y., "The lift and drag forces on a circular cylinder in a flowing fluid," *Proc. Roy. Soc. A*, Vol. 277, 1963, pp. 32-50.